

# Evidence that seismic anisotropy captures upstream palaeo ice fabric: Implications on present day deformation at Whillans Ice Stream, Antarctica

Justin LEUNG,<sup>1</sup> Thomas HUDSON,<sup>1</sup> John-Michael KENDALL,<sup>1</sup> Grace BARCHECK<sup>2</sup>

<sup>1</sup>*Department of Earth Sciences, University of Oxford, Oxford, UK*

<sup>2</sup>*Department of Earth and Atmospheric Sciences, Cornell University, Ithaca, NY, USA*

*Correspondence: Justin Leung <justin.leung@earth.ox.ac.uk>*

**ABSTRACT.** Understanding deformation and slip at ice streams, which are responsible for 90 % of Antarctic ice loss, is vital for accurately modelling large-scale ice flow. Ice crystal orientation fabric (COF) has a first-order effect on ice stream deformation. For the first time, we use shear-wave splitting (SWS) measurements of basal icequakes at Whillans Ice Stream (WIS), Antarctica, to determine a shear-wave anisotropy with an average delay time of 7 ms and fast S-wave polarisation ( $\varphi$ ) of 29.3°. The polarisation is expected to align perpendicular to ice flow, whereas our observation is oblique to the current ice flow direction ( $\sim 280^\circ$ ). This suggests that ice at WIS preserves upstream fabric caused by palaeo-deformation developed over at least the past 450 years, which provides evidence of the concept of Microstructural Fading Memory. Our results imply that changes in the shape of WIS occur on timescales shorter than COF re-equilibration. The “palaeo-fabric” can somewhat control present-day ice flow, which we suggest may somewhat contribute to the long-term slowdown at WIS. Our findings suggest that seismic anisotropy can provide information on past ice sheet dynamics, and how past ice dynamics can play a role in controlling current deformation.

## 25 INTRODUCTION

26 Despite ice streams spanning only 10 % of Antarctica's surface area, they are responsible for 90 % of  
27 Antarctic ice loss (Morgan and others, 1982). Therefore, studying ice stream rheology is important for  
28 understanding Antarctica's contribution to sea-level rise. One source of uncertainty in ice stream dynamics  
29 is the effect of ice fabrics on rheology, where ice with a crystal oriented fabric (COF) can be ten times  
30 weaker in shear in a particular direction relative to isotropic ice (Budd and Jacka, 1989; Pimienta and  
31 others, 1987). Glacial ice is formed of anisotropic grains with hexagonal crystalline symmetry, such that  
32 the viscosity along the basal plane of ice (normal to c-axis) is sixty times less than that perpendicular to  
33 it (Duval and others, 1983). Under stress, the c-axes in a bulk polycrystalline ice mass can rotate to form  
34 an ice COF over timescales of hundreds of years, which can change in response to the stress it encounters  
35 (Azuma, 1994). Hence, understanding ice COF provides insight on past deformation history and how it  
36 might influence future ice flow.

37 Most glacial ice COF measurements are taken from microstructural analyses of ice core samples. How-  
38 ever, these are usually measured from stable or slow-moving regions of ice sheets, and cannot provide much  
39 information of the physical processes in fast-deforming regions (Fan and others, 2021; Llorens and others,  
40 2022). In contrast, seismic anisotropy measurements can be used to deduce ice COF properties over large  
41 areas in different ice settings, including ice streams (Smith and others, 2017). Therefore, seismic anisotropy  
42 can provide insight in these key fast-flowing regions, which can inform models of ice-sheet dynamics.

43 Whillans Ice Stream (WIS) is a major ice stream in West Antarctica that flows into the Ross Sea  
44 embayment (see Figure 1; Picotti and others, 2015). The downstream portion of WIS is known as Whillans  
45 Ice Plain (WIP), and it flows at a speed of over 300 metres per year, with stable sliding of the ice stream  
46 punctuated 1-2 times daily by sudden unstable sliding motion during 30-minute slip events that also  
47 produce high frequency icequakes and tremor (Barcheck and others, 2018; Bindschadler and others, 2003;  
48 Winberry and others, 2013). Long-term slowdown of the ice stream can be seen, with longer periods of  
49 quiescence between slip events over time, suggesting possibility of future stagnation (Winberry and others,  
50 2014). WIS is an excellent area to study basal seismicity given that seismic and global navigation satellite  
51 system data have been collected over recent decades at numerous sites to study its stick-slip cycle (e.g.  
52 Barcheck and others, 2020; Pratt and others, 2014; Walter and others, 2011, 2015; Winberry and others,  
53 2009, 2011) and basal hydrologic cycle (e.g. Fricker and Scambos, 2009; Siegfried and others, 2016).

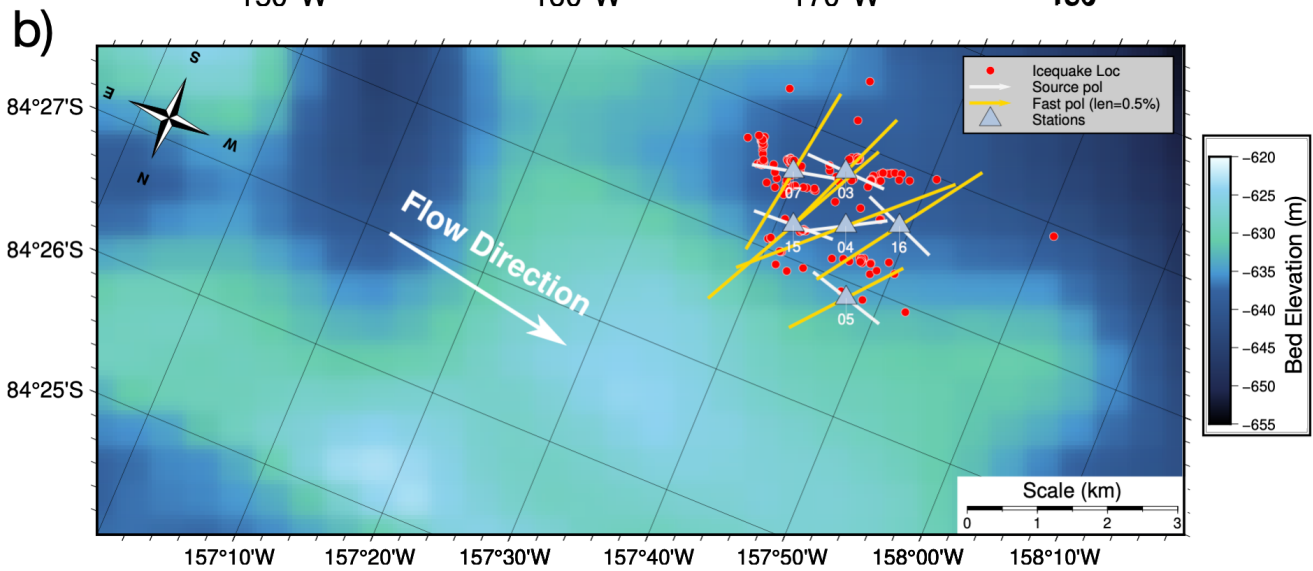
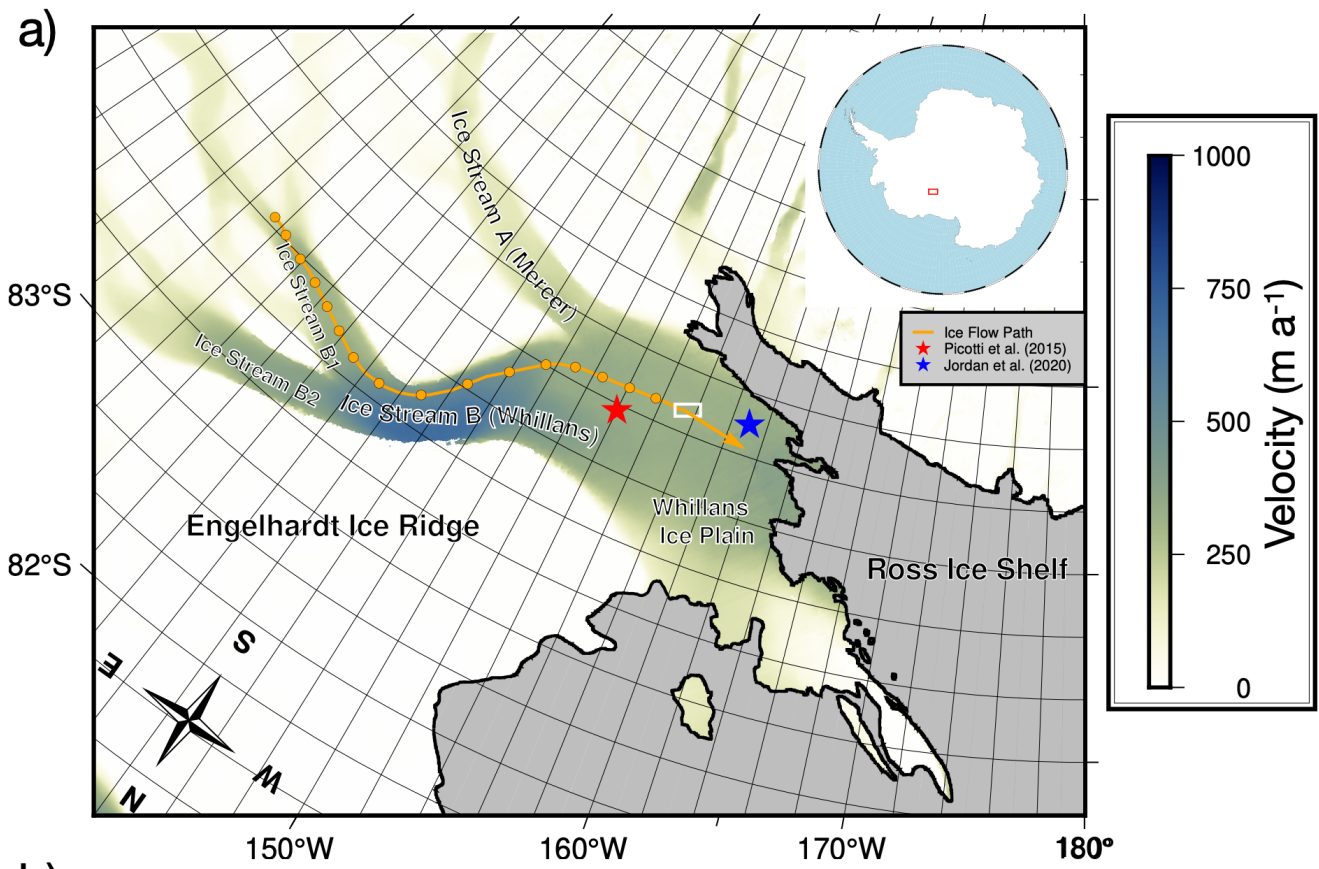


**Fig. 1.** Stereographic maps showing Whillans Ice Stream (WIS) and study location. (a) Regional map of the WIS. The grounding line is marked in the thick black line, and the grey shaded areas mark regions of floating ice. The blue and red star show the study site locations of Jordan and others (2020) and Picotti and others (2015) respectively. The orange line outlines the upstream flow path of the ice at our study site location, assuming current flow velocities, with orange points marking the locations at intervals of 50 years (see supplementary information for flow path calculation). The background colour map shows the ice flow velocity obtained from MEaSURES InSAR-Based Antarctica Ice Velocity Map, Version 2 (Rignot and others, 2017). The study area in (b) is outlined by the white box. (b) Detailed map of the study region. Stations are marked as blue triangles, and icequake locations are shown by red scatter points. Gold lines show the fast S-wave polarisation direction, with the length of the line representing the strength of anisotropy. White lines show the source polarisations for each event, as estimated from recorded shear waves. Dominant ice flow direction (280°) is indicated by the large white arrow. The background colour map shows the bed elevation Morlighem (2022).

There are currently few ice COF observations for the entire ice column at WIS. Picotti and others (2015) used active seismic sources to suggest an azimuth-independent vertically transverse isotropic fabric (VTI) at WIS, with a focus on the top 200 metres. Conversely, Jordan and others (2020) used electromagnetic methods to argue that the c-axes orient parallel to flow at WIS by polarimetric radar sounding that measured the top 400 metres of WIS (see Figure 1 for locations). Here, we provide the first seismic anisotropy measurements from shear-wave splitting of basal icequakes of the entire ice column at Whillans Ice Stream.

## METHODOLOGY

This study uses 319 icequakes recorded between January 20th and February 27th, 2014 by six seismometers at Whillans Ice Plain, Antarctica, part of a network active between 2012 to 2018 (Barcheck and others, 2020; Schwartz, 2012). The ice at the study site is between 690 and 710 m thick (Barcheck and others, 2020) and moving at  $\sim 370 \text{ m a}^{-1}$  (Morlighem, 2022). Since horizontal orientation of the instruments is important for studying seismic anisotropy, we verified the orientation of these instruments using a teleseismic event. We performed a manual search for icequakes focused within the duration of bidaily slip events at WIS, described in Barcheck and others (2021). Icequake arrival times are picked manually and are located using NonLinLoc, a probabilistic non-linear earthquake location algorithm (Lomax and others, 2000). Only icequakes originating at the bed of the ice stream are of interest for measuring total anisotropy in the ice column, therefore icequakes with a source depth shallower than 400 metres are removed. Each icequake is

74 filtered by a 10-100 Hz bandpass filter, based on the dominant source spectra of the icequakes (see Figure  
 75 S1). Seismic anisotropy is analysed on the horizontal (north and east) components because a ~100 m thick  
 76 firn layer refracts the ray path of icequakes to near-vertical incidence at the surface (Picotti and others,  
 77 2015).

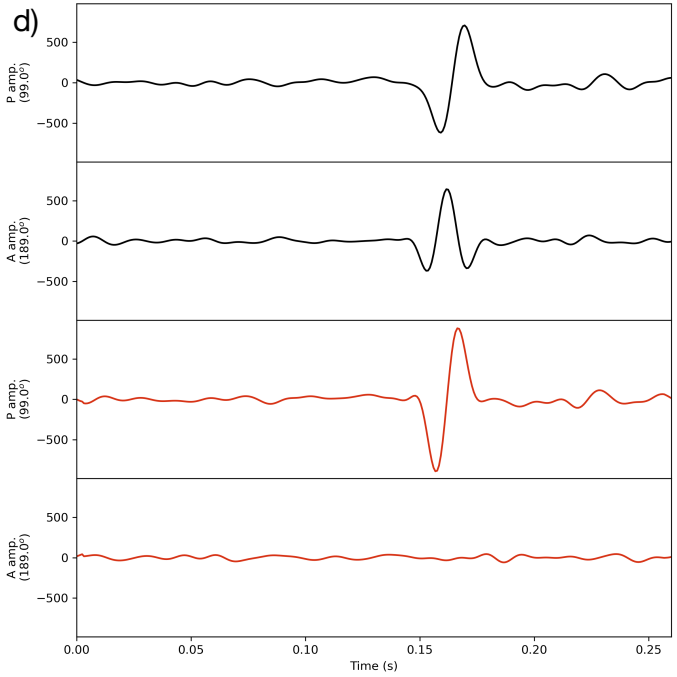
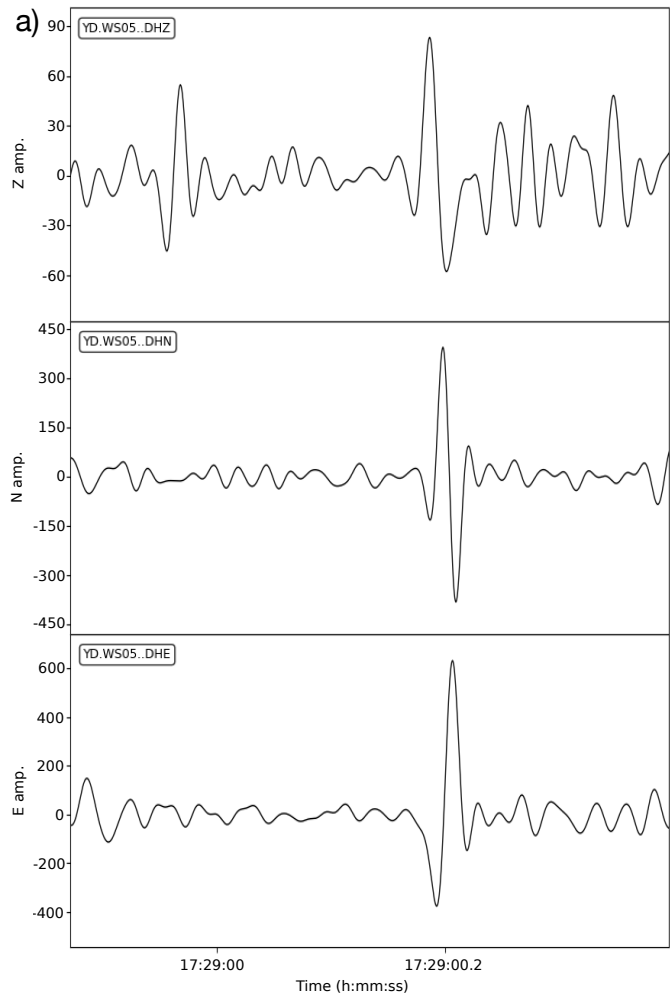
78 Shear-wave splitting (SWS) analysis is conducted using the python package SWSPy (Hudson and  
 79 others, 2023), based on the approach of Wuestefeld and others (2010). It can be summarised as follows:  
 80 First, a range of analysis time windows are defined because SWS measurements are sensitive to window  
 81 lengths (Teanby and others, 2004). Second, a grid search is performed over fast shear-wave polarisation  
 82 of  $-90^\circ < \varphi \leq 90^\circ$  and delay times between fast and slow S-waves of  $0 \leq \delta t \leq 0.1$  for each window, such  
 83 that  $\varphi = 0$  represents a fast shear-wave polarisation in the north (and south) direction. The splitting  
 84 parameters,  $\varphi$  and  $\delta t$ , associated with the minimum second eigenvalue of the S-wave covariance matrix  
 85 that best linearize particle motion, describe the anisotropy observed along a given source-receiver ray path.  
 86 Third, density-based cluster analysis is performed on all optimal  $\varphi$  and  $\delta t$  values, such that the optimal  
 87  $\varphi$  and  $\delta t$  values are obtained from the most stable cluster with minimum variance in  $\varphi$  and  $\delta t$  (Ester and  
 88 others, 1996; Teanby and others, 2004). The source polarisation is then calculated by taking the azimuth  
 89 of the largest eigenvalue of the covariance matrix of the linearised waveforms (Walsh and others, 2013).

90 A well-constrained result after SWS correction is defined as satisfying the following four requirements:  
 91 (1) the particle motion (see Figure 2c) becomes approximately linear after removing splitting using the  
 92 optimal SWS parameters, (2) the error surface (see Figure 2f) has a unique, well-constrained solution, (3)  
 93 splitting parameters ( $\varphi$  and  $\delta t$ ) are stable (see Figure 2e) throughout different clusters, and (4) the quality  
 94 factor  $Q_w$  is larger than 0.7.  $Q_w$  measures the robustness of the splitting measurement, and it is calculated  
 95 by comparing the results from the eigenvalue method of Silver and Chan (1991) to the cross-correlation  
 96 method of Menke and Levin (2003). A value of  $Q_w = 1$  signifies a perfect match between the two methods,  
 97  $Q_w = -1$  a good null result, and  $Q_w = 0$  a poor result (Wuestefeld and others, 2010).

98 The strength of anisotropy ( $\delta V$ ), or the difference between fast and slow S-wave velocities, can be  
 99 quantified by the change in velocity, derived from the delay time ( $\delta t$ ):

$$\delta V = (V \times \delta t \times 100)/r \quad (1)$$

100 where  $V = 1944 \text{ m s}^{-1}$  is the average isotropic shear-wave speed (Smith and others, 2017) and  $r$  the  
 101 source-receiver distance.



Event origin time :  
2014-01-20T17:28:59Z

Station : WS05

$\delta t$  : 0.0064 +/- 0.0008 s

$\phi$  : 36.0° +/- 2.5°

src\_pol: 99.0° +/- 2.8°

Coord. sys. : ZNE

$Q_w$  : 0.984

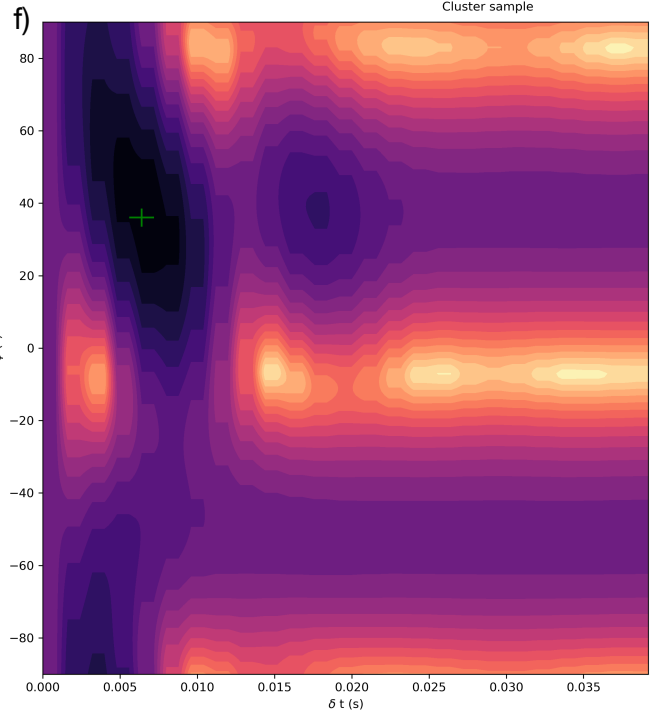
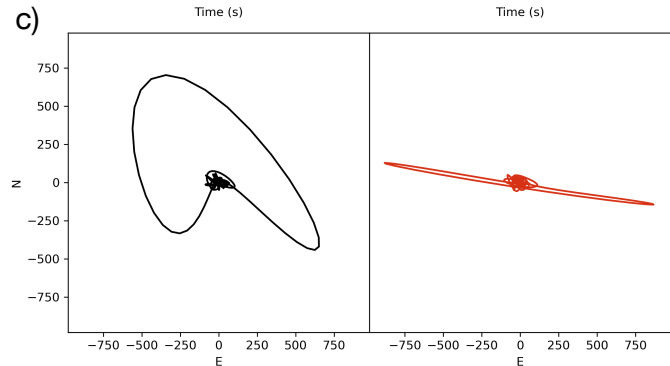
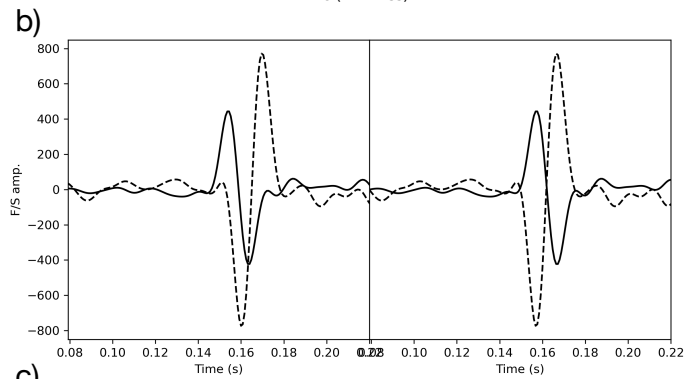
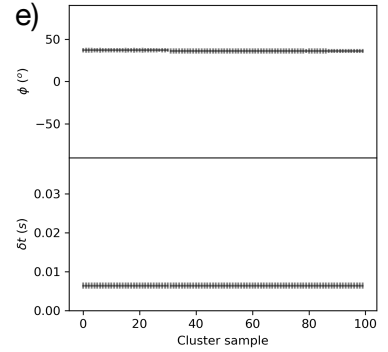




**Fig. 2.** An example of a well-constrained shear-wave splitting event. (a) Icequake signal before correction in the vertical, north and east component. (b) The waveforms before (left) and after (right) SWS correction, plotted in the fast (black line) and slow (dotted) directions. (c) Horizontal (north and east) particle motion before (left) and after (right) SWS correction. (d) Particle motion of icequakes in the source polarisation (P) and the perpendicular azimuth (A) before (top two) and after (bottom two) correction. (e) Optimal  $\varphi$  and  $\delta t$  for different cluster sizes. A good splitting measurement should have constant  $\varphi$  and  $\delta t$  values independent of cluster size. (f) Error surface plotted on  $\varphi$  vs  $\delta t$ . Larger errors are represented with brighter colours, and smaller errors with darker colours. The optimal  $\varphi$  and  $\delta t$  and its uncertainties are shown with the green symbol.

## RESULTS

80 results from 70 events fulfill the aforementioned four criteria, and therefore are chosen for further analysis. The fast S-wave polarisation  $\varphi$  and source polarisation of these events are plotted as polar histograms in Figure 3. For a double-couple icequake source associated with ice slip at the bed, S-wave source polarisation is aligned with the direction of slip (Hudson and others, 2020). One might typically expect the average S-wave source polarisation to align approximately with ice flow direction. Most source polarisation measurements lie approximately in the east-west direction with an average of  $264^\circ\text{N} \pm 22^\circ$  (see Figure 3a), which is in agreement with the Whillans Ice Stream's flow direction of  $280^\circ\text{N} \pm 2^\circ$  (Rignot and others, 2017).

The average delay time for these results is 7.1 ms and ranges from 1.6 ms to 19.2 ms. The average strength of anisotropy,  $\delta V$ , is  $\sim 1.5\%$ , with a maximum of 2.8%. This is below the maximum directional variation in S-wave velocities of single ice crystals of 12% (Lutz and others, 2020).

The shear-wave splitting measurements have an overall mean fast S-wave direction ( $\varphi$ ) of  $29.3^\circ\text{N} \pm 18^\circ$  (see Figure 3b). The uncertainty in this result is defined as one standard deviation, likely representing an upper estimate of uncertainty in the result that could be caused by temporal variations in  $\varphi$  (see Figure S2). Individual receivers generally have mean  $\varphi$  that fall within a range of  $22.4^\circ\text{N}$  to  $47.0^\circ\text{N}$  (see Figure 1b), with the exception of station WS07, which has a mean  $\varphi$  of  $9.1^\circ\text{N}$  (see label 07, Figure 1b). Ice core studies (Lipenkov and others, 1989; Wang and others, 2002; Weikusat and others, 2017) and seismic anisotropy studies (Kufner and others, 2023; Smith and others, 2017) have found that regions of longitudinal extension, such as ice divides and ice streams, have a vertical girdle fabric. In such fabrics,  $\varphi$  is found to be perpendicular to the ice flow direction (Harland and others, 2013). Based on ice flow direction derived from InSAR (Rignot and others, 2017) and the source polarisation data in Figure 3a, one would expect  $\varphi$

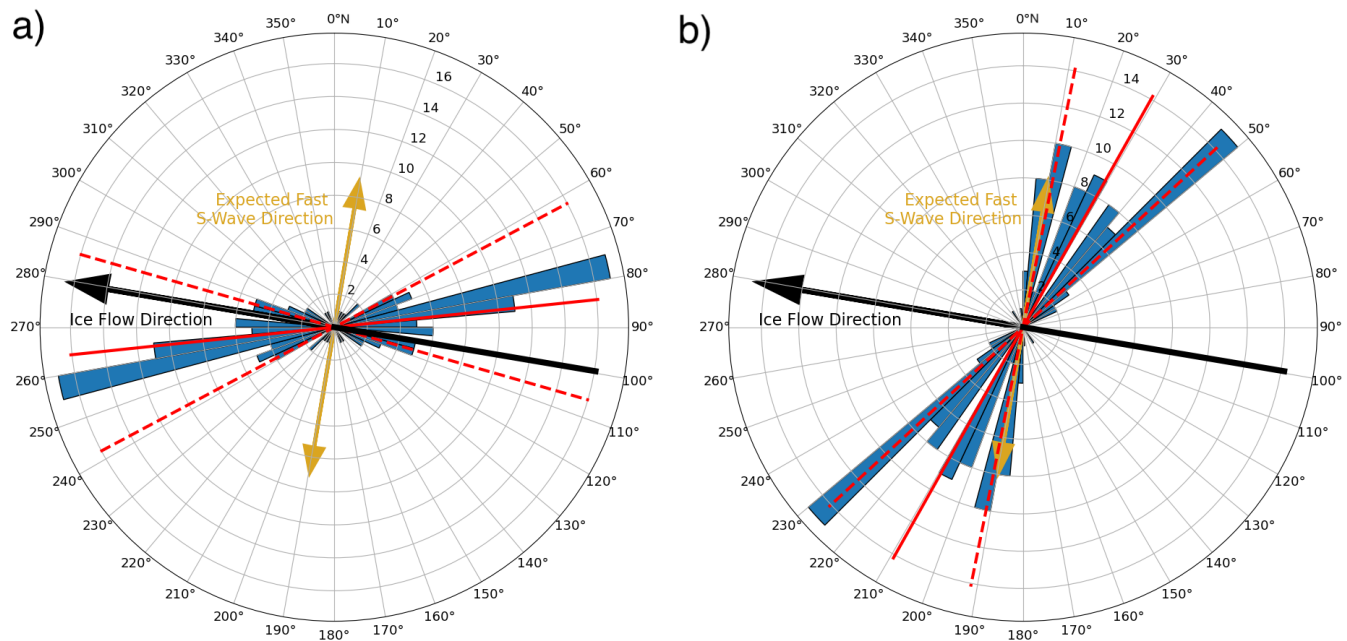


**Fig. 3.** Rose diagrams of (a) source polarisations and (b) fast S-wave directions for all the 80 SWS measurements. The solid and dotted red lines indicate the averages and uncertainties respectively. The gold arrows on both diagrams indicate the expected fast S-wave direction based on ice flow direction, which are shown as black arrows (see main text for further details). Method for estimating uncertainty is included in the supplementary information.

126  $\sim 10^\circ\text{N}$  at the Whillans study site (golden arrow, Figure 3). However, the mean  $\varphi$  we observe of  $29.3^\circ\text{N}$   
 127  $\pm 18^\circ$  is oblique to this expected fast S-wave direction of  $\sim 10^\circ\text{N}$ , even after accounting for uncertainty.  
 128 A t-test shows that the 95 % confidence interval of the fast S-wave directions lies in between  $25.3^\circ\text{N}$  and  
 129  $33.3^\circ\text{N}$  (assuming that the distribution of fast S-wave directions in the data is Gaussian), confirming our  
 130 confidence in this obliquity.



131 **DISCUSSION**132 **Possible origins of an ice COF with an oblique fast S-wave direction**

133 Our results suggest that the ice COF at Whillans Ice Stream (WIS) is oriented oblique, rather than  
134 perpendicular, to the ice flow direction. This obliqueness suggests one of two hypotheses: either that the  
135 local strain at our study site acts oblique to ice flow; or that the ice COF at WIS is the result of preservation  
136 of historic deformation upstream of the study site.

137 Regarding the first hypothesis, a possible reason for extension oblique to ice flow is the differential ice  
138 flux between the two tributaries of Whillans Ice Plain (WIP) across a suture zone. The study site is located  
139 downstream of the confluence between the upper WIS and Mercer Ice Stream (MIS), where the faster flow  
140 of WIS relative to MIS leads to shear strain across the suture zone, which can reorientate ice crystals (see  
141 Figure 4; Beem and others, 2014). However, Bindschadler and others (1987) argue that shear is minimal  
142 between WIS and MIS. Additionally, we postulate that this suture zone has a negligible effect on the ice  
143 COF at our study site because the significant mixing between the two ice streams in the suture zone would  
144 perturb the ice fabric on length scales of the order of hundreds of metres. This mixing would likely yield  
145 significant differences in the fast-polarisation S-wave azimuth ( $\varphi$ ) between the different stations, yet the  
146 fast-polarisation S-wave azimuths remain constant within uncertainty across the network (see Figure 1b)  
147 and a dominant fast polarisation direction can be seen in Figure 3b. Nonetheless, even if our ice COF were  
148 to be affected by this shearing, the suture zone is located upstream of our study site (see high strain rates  
149 near the intersection of WIS and MIS in Figure 4) and therefore also supports the second hypothesis.

150 We instead favour the second hypothesis: that WIS has a “palaeo-COF” that preserves a record of WIS’  
151 upstream palaeo-deformation. Ice core studies and numerical simulations suggest that such preservation  
152 of a palaeo COF is possible (Faria, 2018; Llorens and others, 2022). This can be explained by the concept  
153 of Microstructural Fading Memory, where polycrystalline ice temporarily inherits signatures from its past  
154 microstructure that are progressively erased over a certain relaxation time (Faria, 2018). In the case of  
155 WIS, this past microstructure is the remnant of upstream palaeo-deformation, such that the COF still  
156 has not reoriented towards or re-equilibrated with the local principal compression direction. Most of the  
157 ice deformation at WIP occurs along the shear margins (Truffer and Echelmeyer, 2003) and ice flow is  
158 mainly accommodated by basal sliding, so internal deformation at Whillans is low but still existent. In  
159 such flow regimes, lattice rotation plays an important role relative to dynamic recrystallisation in ice fabric

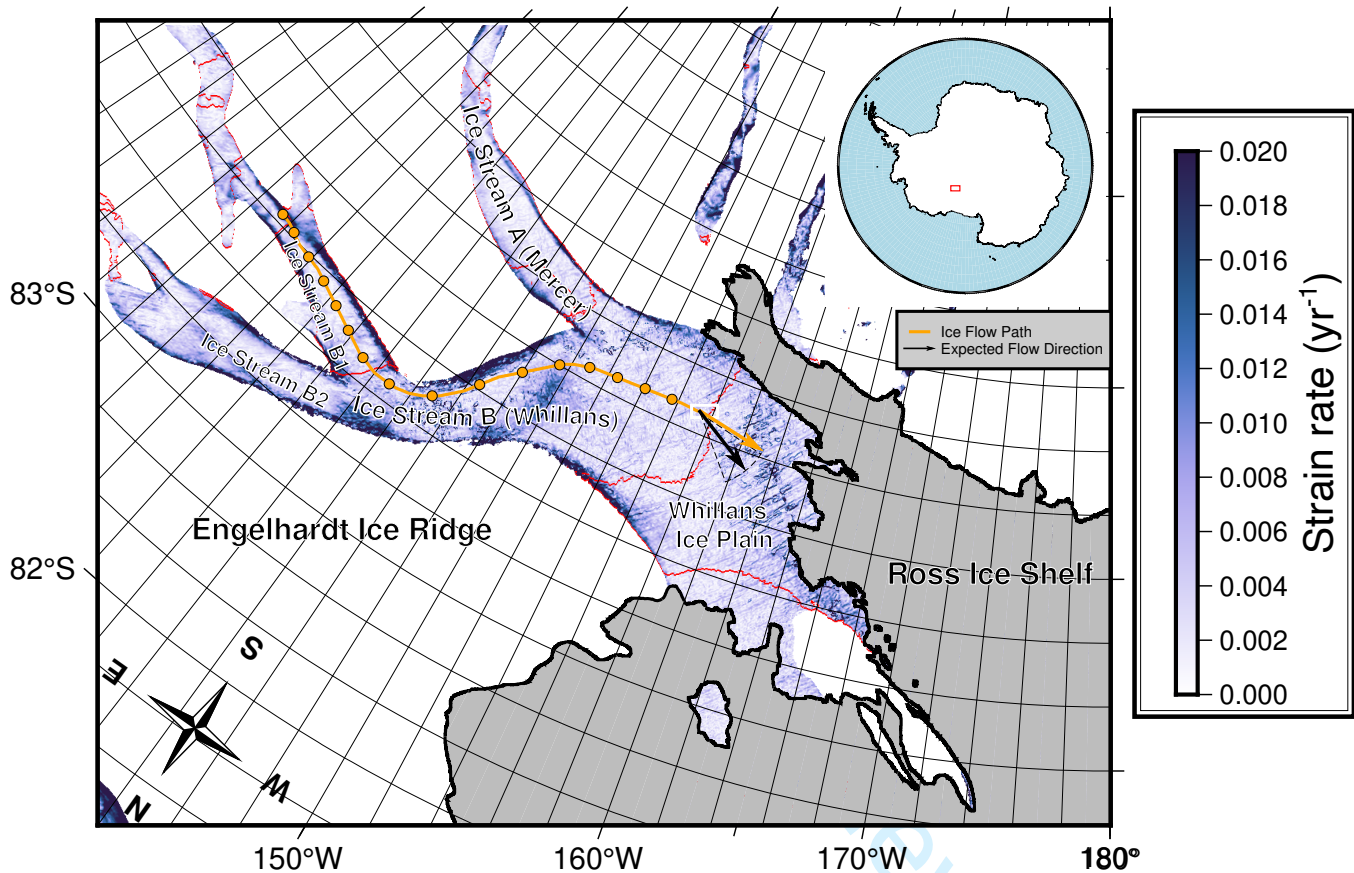


**Fig. 4.** A summary of the study findings. Regions with a flow direction between  $281^{\circ}\text{N}$  to  $317^{\circ}\text{N}$ , are shaded in red. The orange arrow shows the present-day flow direction. The black arrow indicates the flow direction inferred from the fast S-wave polarisation direction, and the dashed black sector outline shows the range of azimuths expressed by the red shaded regions. The background colour map is the strain rate calculated using Rignot and others (2017)'s velocity map (see supplementary information for calculation). Other features shown in this map are as in Figure 1a. The azimuth of the strain rate is shown in Figure S3.

160 evolution (Azuma, 1994; Fan and others, 2021). The c-axes of the ice crystals always rotate towards the  
161 principal direction of compression, which in ice streams is the azimuthal direction perpendicular to the flow  
162 direction (Smith and others, 2017; Thorsteinsson and others, 2003). The meandering nature of WIS alters  
163 the direction of compression, and therefore the ice COF, which we hypothesise in WIS evolves based on c-  
164 axis rotation, represents an integrated history of upstream strain induced by this changing stress. As such,  
165 it is difficult to pinpoint the origin of the fabric formation. However, for the ice COF to have developed  
166 the observed oblique  $\varphi$ , part of the integrated strain history must have originated from upstream areas  
167 in the ice stream where the flow direction was perpendicular to  $\varphi$ . Considering the present-day westward  
168 flow direction only and fast S-wave polarisation uncertainties of  $18^\circ$ , these regions have a flow direction  
169 approximately in the west-northwest direction of  $281^\circ\text{N}$  to  $317^\circ\text{N}$  (see shaded red regions in Figure 4).  
170 The nearest region with such a flow direction along the ice flow path is in the southern tributary of WIS,  
171 indicating that the ice COF could not have been purely derived from the integrated strain alone over the  
172 past 450 years. Consequently, this implies that the entire ice stream flow field of WIS changes on timescales  
173 shorter than ice COF re-equilibration. With this observation, we assumed constant flow directions with  
174 time because ice-flow chronological studies do not suggest major changes in flow direction at WIS over the  
175 past 500 years (Catania and others, 2012). Furthermore, the validity of this assumption does not affect our  
176 conclusion of a palaeo-COF at WIS because present-day ice velocity orientations are insufficient to explain  
177 the observed  $\varphi$ .

178 Larger strain rates can accelerate the rotation of lattices, which reduces the re-equilibration timescales  
179 of ice fabrics and causes the COF to inherit signatures of the local strain field. Therefore, the integrated  
180 strain history better preserves the fabric along flow where the strain is greater. From present-day velocities,  
181 the largest strain rates are located on the main trunk of WIS before it merges with the MIS (see Figure  
182 4). However, these strain rates could have been different in the past because of the dynamic nature of ice  
183 streams. Some studies show that ice streams in the Ross Sea sector have variable mass fluxes over the  
184 past centuries, in particular the Kamb Ice Stream (Bougamont and others, 2015; Catania and others, 2012;  
185 Conway and others, 2002). Further studies of ice anisotropy, in combination with more detailed past ice  
186 conditions and flow calculations, would further evidence any dynamic changes in ice anisotropy along WIS.

187 Given that the expected  $\varphi$  based on current ice flow is only just outside the uncertainty of our results,  
188 we cannot ignore the possibility of an ice COF derived from the present-day study site. However, there  
189 is only a negligible part of the study area that has a flow direction between  $281^\circ\text{N}$  and  $317^\circ\text{N}$ , with the

190 remainder of this region located downstream of the study site (see red shaded regions in Figure 4). Hence,  
191 it is unlikely that enough time elapses for the ice COF to re-equilibrate with the present-day flow direction.  
192 We therefore suggest that the ice fabric is most likely derived from upstream palaeo-deformation.

### 193 **Comparison to other COF studies at WIS**

194 Our results of an oblique fast S-wave direction ( $\varphi$ ) differ from previous findings of an azimuth-independent  
195 fabric (Picotti and others, 2015) and a fabric with  $\varphi$  parallel to flow between 170 m and 400 m depth  
196 (Jordan and others, 2020). We attribute these differences to variations in sampling location and depth (see  
197 Figure 1a).

198 Jordan and others (2020) find two types of vertical girdle fabrics at different depths: a fabric with  $\varphi$   
199 perpendicular to flow for ice up near the surface, and another fabric with  $\varphi$  parallel to flow up to 360  
200 m deep. The former fabric agrees with our results, while the latter suggests a longitudinally compressive  
201 instead of longitudinally extensional stress regime, where compression and extension is defined as the  
202 principal compression axis being parallel and perpendicular to flow respectively. Because their study was  
203 conducted near the grounding line (see Figure 1a), we attribute the second girdle fabric ( $\varphi$  parallel to  
204 flow) to the influence of longitudinal compression due to stronger interactions between the ice and the bed  
205 topography near the grounding zone (Bindschadler and others, 1987; Picotti and others, 2015). If both  
206 fabrics are present in the ice column at our study site, then as we only invert for a single anisotropic layer,  
207 both fabric orientations would be represented as a single, composite result. If two perpendicular fabrics  
208 are present, then any shear-wave splitting measurements would be unable to discriminate between the  
209 layers, with the anisotropy amplitude (delay-time) being damped or amplified, but the overall orientation of  
210 anisotropy remaining constant. Other studies have suggested that the stress regime at WIP is longitudinally  
211 compressive (Bindschadler and others, 1987). However, this likely does not apply to our study site. Firstly,  
212 the strain rates at WIS vary massively as little as 20 kilometres (see Figure 9 of Bindschadler and others,  
213 1987). Secondly, the ice flow path inferred from present-day velocities indicates that the ice at our study site  
214 has travelled along the outer part of the curve at WIP, where we expect the stress regime to be longitudinally  
215 extensional (see Figure 4). Because most of the vertical shear needed to accommodate the driving stress  
216 at WIS occurs within the basal sediment layer (MacAyeal, 1989), we expect the velocity orientation to  
217 be similar across all depths of the ice stream. Thirdly, the ice at our study site is located sufficiently  
218 far from the grounding line, such that it should not experience significant longitudinal compression from

219 interactions between the ice and grounding line bed topography (Pattyn, 2000).

220 Picotti and others (2015) observe an azimuth-independent fabric across the entire ice column, and  
221 suggest that ice streams with low basal shear stress and highly-water-saturated sediments have COF  
222 profiles similar to ice divides due to the increasing influence of vertical compression relative to transverse  
223 compression. However, most of their study is based on surface wave data and travel-time inversions  
224 that could only image the fabric up to 200 m at WIS. Furthermore, their study site is located above  
225 Subglacial Lake Whillans, which is further inwards of the curve at WIP, where the stress regime is less  
226 longitudinally extensional (see Figure 1a). Additionally, their ice COF is likely to have undergone more  
227 equilibration caused by higher strain rates and lower flow velocities on the northern side of WIS (see Figure  
228 4; Bindschadler and others, 1987). Given this variance in ice COF in WIS, future studies of ice deformation  
229 and anisotropy can furthermore reveal the spatial and temporal variability of ice COF at WIS.

### 230 **Comparison to other ice streams**

231 Shear-wave splitting studies from another Antarctic ice stream, Rutford Ice Stream (RIS), find that the  
232 COF at RIS is approximately perpendicular ( $\sim 85^\circ$ ) to ice flow (Harland and others, 2013; Smith and others,  
233 2017). Unlike the deviatoric nature of WIS stream flow, the flow direction at RIS is approximately linear  
234 over COF re-equilibration timescales. As such, it is not possible to discriminate to what extent the COF  
235 at RIS represents the current deformation or a preserved upstream deformation state. Kufner and others  
236 (2023) suggest that the RIS COF signal is dominated by the latter. The strength of anisotropy, effectively  
237 a measure of the strength of the ice COF, at RIS is 3-5 %, while that at WIS is 1.5 %, suggesting that  
238 internal deformation is lower at WIS than RIS. This is consistent with findings that ice flow at WIS is  
239 mainly accommodated by lateral shearing at the margins and basal sliding, where the vertical shear strain  
240 rates required to support the driving stress are mostly confined within a weak basal till layer, and not  
241 within the ice itself (Blankenship and others, 1986; MacAyeal, 1989; Truffer and Echelmeyer, 2003).

242 A recent seismic anisotropy study at RIS by Kufner and others (2023) suggested that multi-layer  
243 anisotropy can be present in ice streams, where the deepest third of the ice stream is thought to comprise an  
244 azimuthally isotropic cluster fabric caused by basal shearing (Azuma, 1994). However, the apparent absence  
245 of multiple fast S-wave phase arrivals in our data suggests that the effects of any multi-layer anisotropy at  
246 WIS are negligible, to which here we define multi-layer anisotropy as a type of depth-dependent anisotropy  
247 with sharper changes in anisotropic signatures with depth. Indeed we did not observe sufficient hints of

248 multi-layer splitting to invert for multiple layers, even though such an inversion is possible at ice streams  
249 (Hudson and others, 2023). Inverting for a multi-layer anisotropic model at WIS would introduce additional  
250 parameters on layer thicknesses and fast polarisation directions, which could result in overfitting of the  
251 data, compared to a single depth-integrated anisotropy model.

252 Because most of the vertical shear at WIS is accommodated within the basal sediment layer (MacAyeal,  
253 1989), we would expect the surface velocity direction to represent the orientation of maximum strain with  
254 depth, except perhaps for a thin (1 to 10s metres) basal shear layer near the ice-bed interface, which could  
255 vary somewhat in orientation over short length scales (10s to 100s metres) due to local bed topography  
256 variations. The depth of ice affected by shearing will either be too thin to be observed in seismic lengthscales  
257 or too weak to affect the overall anisotropic signature of the ice stream (Bindschadler and others, 1987;  
258 Blankenship and others, 1986). Additionally, even if the shear zone were to exhibit strong anisotropy, the  
259 cluster fabric that would likely result is azimuthally isotropic and therefore has little effect on our results of  
260 a preferred c-axis azimuth. In summary, we therefore would expect the dominant anisotropy to be oriented  
261 relative to surface ice flow velocity.

## 262 **Implications of an oblique ice fabric on ice flow**

263 The effective viscosity for compression and extension is higher along the basal plane. As seen in RIS, where  
264 the horizontal c-axis is oriented perpendicular to flow, the effective viscosity is higher along flow than across  
265 flow (Jordan and others, 2022; Kufner and others, 2023). This hardening along the flow direction, which  
266 is perpendicular to the c-axes and parallel to the basal plane, is thought to increase the viscosity by an  
267 order of magnitude relative to isotropic ice (Kufner and others, 2023). However, our results at WIS show  
268 a c-axis orientation that is not perpendicular, but oblique to ice flow or equivalently a misalignment of  
269 the basal plane with the flow direction. Because the basal plane is associated with directions of highest  
270 effective viscosity, this misalignment implies that internal deformation will be resisted more at WIS if the  
271 c-axis direction re-equilibrates with the local principal stress direction. The internal deformation in WIS  
272 might be minimal today, but it may become important in the future. Firstly, the long-term slowdown  
273 in WIS has been associated with basal strengthening, especially in the upper portion of the ice stream  
274 (Beem and others, 2014). If the driving stress is somehow sustained, then a lower proportion of this stress  
275 could be accommodated by the basal till and a higher proportion through internal deformation. Secondly,  
276 the deceleration results in increased duration between periods of slip events at WIS, which is expected to



277 increase the significance of internal viscous deformation (Winberry and others, 2014).

278 Our observations also suggest that palaeo ice COF can somewhat control present-day ice flow. If  
279 the shape of an ice stream deviates on length scales less than the distance ice travels within the COF  
280 re-equilibration time, then the COF may not be aligned with ice flow, limiting the effective viscosity of  
281 the ice column along the ice flow direction. If an ice stream flows linearly for a duration greater than  
282 the re-equilibration time, then the COF should re-equilibrate with the bulk stress, such that the basal  
283 plane will rotate closer to the ice flow direction, increase the effective viscosity, and decrease the rate of  
284 deformation downstream. The degree of re-equilibration of an ice COF with the surrounding stresses is  
285 not only dependent on ice stream shape, but also on flow speed. Slower-flowing ice will have more time  
286 to re-equilibrate with the surrounding stress field. The long-term slowdown at WIS can therefore provide  
287 more time for its ice COF re-equilibration, which reduces the misalignment of the basal plane with flow  
288 direction and increases the effective viscosity along the flow direction of WIS. Despite internal deformation  
289 becoming more significant with the long-term slowdown, this higher effective viscosity instead indicates  
290 that internal deformation will be more difficult, which has consequences on future predictions of the ice  
291 flow at WIS.

292 Most icesheet-scale ice dynamics models assume either that ice is isotropic, or parameterise anisotropy  
293 effects via an enhancement factor to account for ice weakening due to COF orientation relative to ice  
294 flow. However, recent studies such as Smith and others (2017) and Kufner and others (2023), suggest that  
295 enhancement factors should no longer be used to parameterise ice viscosity in fast-deforming regions such  
296 as ice streams. Additionally, the effect of anisotropy on the viscosity of ice can differ significantly between  
297 different types of ice fabrics. Most results concluding that ice weakens when anisotropy is considered  
298 originate from studies based on cluster fabrics. Conversely, radar and seismic observations at RIS (Jordan  
299 and others, 2022; Kufner and others, 2023), and numerical simulations (Ma and others, 2010) show that  
300 ice with a girdle COF has a higher effective viscosity in relation to isotropic ice. Our findings at WIS  
301 further support the importance of characterising COF- and directionally-dependent ice viscosity in ice flow  
302 models, and emphasise that understanding ice COF in both space and time is important for producing  
303 more realistic deformation in ice dynamics models.

## 304 CONCLUSION

305 This study provides shear-wave splitting (SWS) observations from basal icequakes at Whillans Ice Stream  
306 (WIS). From these observations, we infer the ice crystal orientation fabric (COF) anisotropy over the entire  
307 ice column. The observations provide insight into past and present deformation at WIS. The results from  
308 80 discrete icequakes SWS observations show that WIS has an average fast S-wave direction ( $\varphi$ ) of 29.3°,  
309 which is oblique to the expected direction of  $\sim 10^\circ$  based on ice flow direction at the study site of around  
310 280°. We suggest that the ice COF records an integrated strain history along its flow path for at least the  
311 past 450 years to have preserved deformation in the direction of  $\varphi$ , and therefore evidence the concept of  
312 Microstructural Fading Memory. The non-perpendicularity of  $\varphi$  to ice flow implies that the shape of an  
313 ice stream can affect its flow, such that spatially deviatoric ice streams including WIS can flow slower if  
314 they were instead linear. Given the long-term slowdown of WIS, the basal plane will have more time to  
315 re-equilibrate with the surrounding stress field, which can further contribute to the long-term slowdown.  
316 Our results have implications for ice sheet models, suggesting that historic ice flow can preserve ice fabric  
317 and hence directionally-dependent ice viscosity that might play an important role in such models.

## 318 SUPPLEMENTARY MATERIAL

319 The supplementary material for this article can be found in `suppl_mat_WIS_anisotropy.pdf`, as attached  
320 with the submission of this manuscript.

## 321 ACKNOWLEDGEMENTS

322 We thank Alex Brisbourne for his comments, which have improved the manuscript.

## 323 REFERENCES

- 324 Azuma N (1994) A flow law for anisotropic ice and its application to ice sheets. *Earth and Planetary Science Letters*,  
325 **128**(3-4), 601–614, ISSN 0012821X (doi: 10.1016/0012-821X(94)90173-2)
- 326 Barcheck CG, Tulaczyk S, Schwartz SY, Walter JI and Winberry JP (2018) Implications of basal micro-earthquakes  
327 and tremor for ice stream mechanics: Stick-slip basal sliding and till erosion. *Earth and Planetary Science Letters*,  
328 **486**, 54–60, ISSN 0012821X (doi: 10.1016/j.epsl.2017.12.046)
- 329 Barcheck CG, Schwartz SY and Tulaczyk S (2020) Icequake streaks linked to potential mega-scale glacial lineations  
330 beneath an Antarctic ice stream. *Geology*, **48**(2), 99–102, ISSN 0091-7613, 1943-2682 (doi: 10.1130/G46626.1)
- 331 Barcheck G, Brodsky EE, Fulton PM, King MA, Siegfried MR and Tulaczyk S (2021) Migratory earthquake precursors  
332 are dominant on an ice stream fault. *Sci. Adv.*, **7**(6), eabd0105, ISSN 2375-2548 (doi: 10.1126/sciadv.abd0105)
- 333 Beem LH, Tulaczyk SM, King MA, Bougamont M, Fricker HA and Christoffersen P (2014) Variable deceleration  
334 of Whillans Ice Stream, West Antarctica. *J. Geophys. Res. Earth Surf.*, **119**(2), 212–224, ISSN 21699003 (doi:  
335 10.1002/2013JF002958)
- 336 Bindschadler RA, Stephenson SN, MacAyeal DR and Shabtaie S (1987) Ice dynamics at the mouth of ice stream B,  
337 Antarctica. *J. Geophys. Res.*, **92**(B9), 8885, ISSN 0148-0227 (doi: 10.1029/JB092iB09p08885)
- 338 Bindschadler RA, King MA, Alley RB, Anandakrishnan S and Padman L (2003) Tidally controlled stick-slip discharge  
339 of a West Antarctic ice. *Science*, **301**(5636), 1087–1089
- 340 Blankenship DD, Bentley CR, Rooney ST and Alley RB (1986) Seismic measurements reveal a saturated porous  
341 layer beneath an active Antarctic ice stream. *Nature*, **322**(6074), 54–57, ISSN 0028-0836, 1476-4687 (doi:  
342 10.1038/322054a0)
- 343 Bougamont M, Christoffersen P, Price SF, Fricker HA, Tulaczyk S and Carter SP (2015) Reactivation of Kamb Ice  
344 Stream tributaries triggers century-scale reorganization of Siple Coast ice flow in West Antarctica. *Geophysical*  
345 *Research Letters*, **42**(20), 8471–8480, ISSN 0094-8276, 1944-8007 (doi: 10.1002/2015GL065782)
- 346 Budd W and Jacka T (1989) A review of ice rheology for ice sheet modelling. *Cold Regions Science and Technology*,  
347 **16**(2), 107–144, ISSN 0165232X (doi: 10.1016/0165-232X(89)90014-1)
- 348 Catania G, Hulbe C, Conway H, Scambos T and Raymond C (2012) Variability in the mass flux of the Ross ice  
349 streams, West Antarctica, over the last millennium. *J. Glaciol.*, **58**(210), 741–752, ISSN 0022-1430, 1727-5652  
350 (doi: 10.3189/2012JoG11J219)

- 351 Conway H, Catania G, Raymond CF, Gades AM, Scambos TA and Engelhardt H (2002) Switch of flow direction in  
352 an Antarctic ice stream. *Nature*, **419**(6906), 465–467, ISSN 0028-0836, 1476-4687 (doi: 10.1038/nature01081)
- 353 Duval P, Ashby MF and Anderman I (1983) Rate-controlling processes in the creep of polycrystalline ice. *J. Phys.*  
354 *Chem.*, **87**(21), 4066–4074, ISSN 0022-3654, 1541-5740 (doi: 10.1021/j100244a014)
- 355 Ester M, Kriegel HP, Sander J and Xu X (1996) A density-based algorithm for discovering clusters in large spatial  
356 databases with noise. In *Proceedings of the Second International Conference on Knowledge Discovery and Data*  
357 *Mining*, KDD'96, 226–231, AAAI Press, place: Portland, Oregon
- 358 Fan S, Cross AJ, Prior DJ, Goldsby DL, Hager TF, Negrini M and Qi C (2021) Crystallographic Preferred Orientation  
359 (CPO) Development Governs Strain Weakening in Ice: Insights From High-Temperature Deformation Experiments.  
360 *JGR Solid Earth*, **126**(12), e2021JB023173, ISSN 2169-9313, 2169-9356 (doi: 10.1029/2021JB023173)
- 361 Faria SH (2018) Slip-band distributions and microstructural fading memory beneath the firn–ice transition of polar ice  
362 sheets. *Mechanics Research Communications*, **94**, 95–101, ISSN 00936413 (doi: 10.1016/j.mechrescom.2018.09.009)
- 363 Fricker HA and Scambos T (2009) Connected subglacial lake activity on lower Mercer and Whillans Ice  
364 Streams, West Antarctica, 2003–2008. *J. Glaciol.*, **55**(190), 303–315, ISSN 0022-1430, 1727-5652 (doi:  
365 10.3189/002214309788608813)
- 366 Harland S, Kendall JM, Stuart G, Lloyd G, Baird A, Smith A, Pritchard H and Brisbourne A (2013) Deformation  
367 in Rutford Ice Stream, West Antarctica: measuring shear-wave anisotropy from icequakes. *Ann. Glaciol.*, **54**(64),  
368 105–114, ISSN 0260-3055, 1727-5644 (doi: 10.3189/2013AoG64A033)
- 369 Hudson TS, Brisbourne AM, Walter F, Gräff D, White RS and Smith AM (2020) Icequake Source Mechanisms  
370 for Studying Glacial Sliding. *JGR Earth Surface*, **125**(11), e2020JF005627, ISSN 2169-9003, 2169-9011 (doi:  
371 10.1029/2020JF005627)
- 372 Hudson TS, Asplet J and Walker AM (2023) Automated shear-wave splitting analysis for single- and multi- layer  
373 anisotropic media. *Seismica*, **2**(2), ISSN 2816-9387 (doi: 10.26443/seismica.v2i2.1031)
- 374 Jordan TM, Schroeder DM, Elsworth CW and Siegfried MR (2020) Estimation of ice fabric within Whillans Ice  
375 Stream using polarimetric phase-sensitive radar sounding. *Ann. Glaciol.*, **61**(81), 74–83, ISSN 0260-3055, 1727-  
376 5644 (doi: 10.1017/aog.2020.6)
- 377 Jordan TM, Martín C, Brisbourne AM, Schroeder DM and Smith AM (2022) Radar Characterization of Ice Cryst-  
378 tal Orientation Fabric and Anisotropic Viscosity Within an Antarctic Ice Stream. *JGR Earth Surface*, **127**(6),  
379 e2022JF006673, ISSN 2169-9003, 2169-9011 (doi: 10.1029/2022JF006673)

- 380 Kufner S, Wookey J, Brisbourne AM, Martín C, Hudson TS, Kendall JM and Smith AM (2023) Strongly Depth-  
381 Dependent Ice Fabric in a Fast-Flowing Antarctic Ice Stream Revealed With Icequake Observations. *JGR Earth*  
382 *Surface*, **128**(3), e2022JF006853, ISSN 2169-9003, 2169-9011 (doi: 10.1029/2022JF006853)
- 383 Lipenkov V, Barkov N, Duval P and Pimienta P (1989) Crystalline Texture of the 2083 m Ice Core at Vostok Station,  
384 Antarctica. *J. Glaciol.*, **35**(121), 392–398, ISSN 0022-1430, 1727-5652 (doi: 10.3189/S0022143000009321)
- 385 Llorens MG, Griera A, Bons PD, Weikusat I, Prior DJ, Gomez-Rivas E, De Riese T, Jimenez-Munt I, García-  
386 Castellanos D and Lebensohn RA (2022) Can changes in deformation regimes be inferred from crystallographic  
387 preferred orientations in polar ice? *The Cryosphere*, **16**(5), 2009–2024, ISSN 1994-0424 (doi: 10.5194/tc-16-2009-  
388 2022)
- 389 Lomax A, Virieux J, Volant P and Berge-Thierry C (2000) Probabilistic Earthquake Location in 3D and Layered  
390 Models. In CH Thurber and N Rabinowitz (eds.), *Advances in Seismic Event Location*, 101–134, Springer Nether-  
391 lands, Dordrecht, ISBN 978-94-015-9536-0 (doi: 10.1007/978-94-015-9536-0\_5)
- 392 Lutz F, Eccles J, Prior DJ, Craw L, Fan S, Hulbe C, Forbes M, Still H, Pyne A and Mandeno D (2020) Constraining  
393 Ice Shelf Anisotropy Using Shear Wave Splitting Measurements from Active-Source Borehole Seismics. *JGR Earth*  
394 *Surface*, **125**(9), e2020JF005707, ISSN 2169-9003, 2169-9011 (doi: 10.1029/2020JF005707)
- 395 Ma Y, Gagliardini O, Ritz C, Gillet-Chaulet F, Durand G and Montagnat M (2010) Enhancement factors for  
396 grounded ice and ice shelves inferred from an anisotropic ice-flow model. *J. Glaciol.*, **56**(199), 805–812, ISSN  
397 0022-1430, 1727-5652 (doi: 10.3189/002214310794457209)
- 398 MacAyeal DR (1989) Large-scale ice flow over a viscous basal sediment: Theory and application to ice stream B,  
399 Antarctica. *J. Geophys. Res.*, **94**(B4), 4071–4087, ISSN 0148-0227 (doi: 10.1029/JB094iB04p04071)
- 400 Menke W and Levin V (2003) The cross-convolution method for interpreting *SKS* splitting observations, with appli-  
401 cation to one and two-layer anisotropic earth models. *Geophysical Journal International*, **154**(2), 379–392, ISSN  
402 0956540X, 1365246X (doi: 10.1046/j.1365-246X.2003.01937.x)
- 403 Morgan V, Jacka T, Akerman G and Clarke A (1982) Outlet Glacier and Mass-Budget Studies in Enderby,  
404 Kemp, and Mac. Robertson Lands, Antarctica. *Ann. Glaciol.*, **3**, 204–210, ISSN 0260-3055, 1727-5644 (doi:  
405 10.3189/S0260305500002780)
- 406 Morlighem M (2022) MEaSUREs BedMachine Antarctica, Version 3 (doi: 10.5067/FPSU0V1MWUB6)
- 407 Pattyn F (2000) Ice-sheet modelling at different spatial resolutions: focus on the grounding zone. *Ann. Glaciol.*, **31**,  
408 211–216, ISSN 0260-3055, 1727-5644 (doi: 10.3189/172756400781820435)

- 409 Picotti S, Vuan A, Carcione JM, Horgan HJ and Anandakrishnan S (2015) Anisotropy and crystalline fabric of  
410 Whillans Ice Stream (West Antarctica) inferred from multicomponent seismic data. *JGR Solid Earth*, **120**(6),  
411 4237–4262, ISSN 2169-9313, 2169-9356 (doi: 10.1002/2014JB011591)
- 412 Pimienta P, Duval P and Lipenkov VY (1987) Mechanical behavior of anisotropic polar ice. In *Proceedings of the*  
413 *Vancouver Symposium*, volume 170, 57–66, International Association of Hydrological Sciences
- 414 Pratt MJ, Winberry JP, Wiens DA, Anandakrishnan S and Alley RB (2014) Seismic and geodetic evidence for  
415 grounding-line control of Whillans Ice Stream stick-slip events: Whillans Ice Stream Stick-Slip Events. *J. Geophys.*  
416 *Res. Earth Surf.*, **119**(2), 333–348, ISSN 21699003 (doi: 10.1002/2013JF002842)
- 417 Rignot E, Mouginit J, Morlighem M and Scheuchl B (2017) MEaSUREs InSAR-Based Antarctica Ice Velocity Map,  
418 Version 2 (doi: 10.5067/D7GK8F5J8M8R)
- 419 Schwartz SY (2012) Whillans Ice Stream Subglacial Access Research Drilling (doi: 10.7914/SN/YD\_2012)
- 420 Siegfried MR, Fricker HA, Carter SP and Tulaczyk S (2016) Episodic ice velocity fluctuations triggered by a sub-  
421 glacial flood in West Antarctica. *Geophysical Research Letters*, **43**(6), 2640–2648, ISSN 0094-8276, 1944-8007 (doi:  
422 10.1002/2016GL067758)
- 423 Smith EC, Baird AF, Kendall JM, Martín C, White RS, Brisbourne AM and Smith AM (2017) Ice fabric in an  
424 Antarctic ice stream interpreted from seismic anisotropy. *Geophysical Research Letters*, **44**(8), 3710–3718, ISSN  
425 0094-8276, 1944-8007 (doi: 10.1002/2016GL072093)
- 426 Teanby NA, Kenda NA, Kendall JM, Martin C, White RS, Brisbourne AM and Smith AM (2004) Automation  
427 of Shear-Wave Splitting Measurements using Cluster Analysis. *Bulletin of the Seismological Society of America*,  
428 **94**(2), 453–463, ISSN 0037-1106 (doi: 10.1785/0120030123)
- 429 Thorsteinsson T, Waddington ED and Fletcher RC (2003) Spatial and temporal scales of anisotropic effects in  
430 ice-sheet flow. *Ann. Glaciol.*, **37**, 40–48, ISSN 0260-3055, 1727-5644 (doi: 10.3189/172756403781815429)
- 431 Truffer M and Echelmeyer KA (2003) Of isbræ and ice streams. *Ann. Glaciol.*, **36**, 66–72, ISSN 0260-3055, 1727-5644  
432 (doi: 10.3189/172756403781816347)
- 433 Walsh E, Arnold R and Savage MK (2013) Silver and Chan revisited: SILVER AND CHAN REVISITED. *J. Geophys.*  
434 *Res. Solid Earth*, **118**(10), 5500–5515, ISSN 21699313 (doi: 10.1002/jgrb.50386)
- 435 Walter JI, Brodsky EE, Tulaczyk S, Schwartz SY and Pettersson R (2011) Transient slip events from near-field seismic  
436 and geodetic data on a glacier fault, Whillans Ice Plain, West Antarctica: RUPTURE SPEEDS ON WHILLANS  
437 ICE PLAIN. *J. Geophys. Res.*, **116**(F1), n/a–n/a, ISSN 01480227 (doi: 10.1029/2010JF001754)



- 438 Walter JI, Svetlizky I, Fineberg J, Brodsky EE, Tulaczyk S, Grace Barcheck C and Carter SP (2015) Rupture speed  
439 dependence on initial stress profiles: Insights from glacier and laboratory stick-slip. *Earth and Planetary Science*  
440 *Letters*, **411**, 112–120, ISSN 0012821X (doi: 10.1016/j.epsl.2014.11.025)
- 441 Wang Y, Thorsteinsson T, Kipfstuhl J, Miller H, Dahl-Jensen D and Shoji H (2002) A vertical girdle fabric in  
442 the NorthGRIP deep ice core, North Greenland. *Ann. Glaciol.*, **35**, 515–520, ISSN 0260-3055, 1727-5644 (doi:  
443 10.3189/172756402781817301)
- 444 Weikusat I, Jansen D, Binder T, Eichler J, Faria SH, Wilhelms F, Kipfstuhl S, Sheldon S, Miller H, Dahl-Jensen D and  
445 Kleiner T (2017) Physical analysis of an Antarctic ice core—towards an integration of micro- and macrodynamics of  
446 polar ice. *Phil. Trans. R. Soc. A.*, **375**(2086), 20150347, ISSN 1364-503X, 1471-2962 (doi: 10.1098/rsta.2015.0347)
- 447 Winberry JP, Anandakrishnan S, Alley RB, Bindschadler RA and King MA (2009) Basal mechanics of ice streams:  
448 Insights from the stick-slip motion of Whillans Ice Stream, West Antarctica. *J. Geophys. Res.*, **114**(F1), F01016,  
449 ISSN 0148-0227 (doi: 10.1029/2008JF001035)
- 450 Winberry JP, Anandakrishnan S, Wiens DA, Alley RB and Christianson K (2011) Dynamics of stick-slip motion,  
451 Whillans Ice Stream, Antarctica. *Earth and Planetary Science Letters*, **305**(3-4), 283–289, ISSN 0012821X (doi:  
452 10.1016/j.epsl.2011.02.052)
- 453 Winberry JP, Anandakrishnan S, Wiens DA and Alley RB (2013) Nucleation and seismic tremor associated with  
454 the glacial earthquakes of Whillans Ice Stream, Antarctica. *Geophysical Research Letters*, **40**(2), 312–315, ISSN  
455 0094-8276, 1944-8007 (doi: 10.1002/grl.50130)
- 456 Winberry JP, Anandakrishnan S, Alley RB, Wiens DA and Pratt MJ (2014) Tidal pacing, skipped slips and the  
457 slowdown of Whillans Ice Stream, Antarctica. *J. Glaciol.*, **60**(222), 795–807, ISSN 0022-1430, 1727-5652 (doi:  
458 10.3189/2014JoG14J038)
- 459 Wuestefeld A, Al-Harrasi O, Verdon JP, Wookey J and Kendall JM (2010) A strategy for automated analysis of  
460 passive microseismic data to image seismic anisotropy and fracture characteristics: A strategy for automated anal-  
461 ysis of passive microseismic data. *Geophysical Prospecting*, **58**(5), 755–773, ISSN 00168025 (doi: 10.1111/j.1365-  
462 2478.2010.00891.x)